International Journal of Applied Mechanics
Vol. 3, No. 1 (2011) 21–46

DOI: 10.1142/S1758825111000853

Imperial College Press
www.icpress.co.uk

EIGENVALUE ANALYSIS OF THIN PLATE WITH COMPLICATED SHAPES BY A NOVEL MESH-FREE METHOD

TINH QUOC BUI*

Department of Civil Engineering, University of Siegen
Paul-Bonatz-Strasse 9-11, Siegen D-57076, Germany
bui-quoc@bauwesen.uni-siegen.de

MINH NGOC NGUYEN

Department of Civil Engineering
Ruhr University Bochum, University Street
150 Bochum City, 44801, Germany

Received 12 June 2010
Accepted 27 September 2010

Further development of a novel mesh-free method for eigenvalue analysis of thin plate structures with complicated shapes is presented in this paper. A mesh-free method used the moving Kriging interpolation technique for constructing the shape functions, which possess the Kronecker's delta property, is formulated. Thus, it makes the present method efficient in enforcing the essential boundary conditions and none of any special techniques are required. The present plate theory followed the classical Kirchhoff's assumption and the deflection is in general approximated through the moving Kriging interpolation. Also, the mesh-free formulations for the vibration problem are formed in a simple way as finite element methods. The orthogonal transformation technique is used to implement the essential boundary conditions in the eigenvalue equation. A standard weak form is adopted to discrete the governing partial differential equation of plates. Some numerical examples are attempted to demonstrate the applicability, the effectiveness, and the accuracy of the method.

Keywords: Mesh-free; plate; frequency; vibration; moving Kriging interpolation.

1. Introduction

Plate structures usually play an important role in a variety of structural mechanics. The applications of such plates generally are of great importance and usefulness in reality. Normally, finding an exact solution for these plate structures by analytical approaches is obviously very difficult. Due to significant advantages of the computers and numerical methods one now tends to find an approximate solution rather than the exact one. However, they are always in great demand by the engineering inherent discipline. Numerical methods such as finite element methods (FEM)

*Corresponding author.

have been successfully applied to analyze thin structures. However, it is not easy to conveniently construct conformable plate element, i.e., C^1 consistency of higher order as required for thin plates. Among the numerical methods, the extended finite element method (X-FEM) was recently proposed by Belytschko and Black [1999] and soon after promoted by Moes *et al.* [1999] by substantially adding an appropriate enrichment function into the traditional finite element approximation function in terms of the concept of partition of unity introduced by Melenk and Babuska [1996]. The X-FEM is mainly aimed to model discontinuities. Also, a new class of mesh-free methods [Atluri, 2004; Atluri *et al.*, 1998; Belytschko *et al.*, 1994; Liu, 2003; Li and Liu, 2004] has emerged as an alternative way for solving partial differential equations using a set of scattered nodes in the problem domain regardless of "element" or "mesh". It has been extensively used for many different problems in engineering. However, most recent mesh-free methods have the same problem of the lack of the Kronecker's delta property. This evidently leads to a difficulty in the enforcement of the essential boundary conditions.

Thus, it is easily seen that many efforts have been devoted in order to eliminate the difficulty in enforcing the boundary condition in various ways such as Lagrange multipliers [Belytschko *et al.*, 1994], penalty method [Liu, 2003], coupling with the FEM [Belyschko *et al.*, 1995], etc. The present study is a further development from previous works [Bui *et al.*, 2009], for free vibration analysis of classical plates using the meshless moving Kriging interpolation method. One of the superior advantage of the present method over the conventional methods, e.g., moving least-square approximation, is that the capability of getting rid of such drawback of imposing the boundary conditions. In other words, most mesh-free methods have developed based on the displacement-based approaches. In contrast, an equilibrium-based mesh-free model based on a stress approach has been developed for elastic problems [Duflot *et al.*, 2002; Bui, 2005; Bui *et al.*, 2006].

A large number of studies accounted for plate structures have been reported. They can easily be found in the literature and some of them are reviewed as follows: the authors recently used the method to static flexural investigation of Kirchhoff plates [Bui *et al.*, 2009]. Krysl and Belytschko [1995] extended the element-free Galerkin method to static analysis of thin plates. Liu and Chen [2001] further applied the element-free Galerkin (EFG) method to static and free vibration analyses of thin plates with complicated shapes. Chen *et al.* [2004] proposed a meshless method accounted for the free vibration analysis of circular and rectangular clamped plates using radial basis function. Liu *et al.* [2006] developed the mesh-free Hermite-type radial point interpolation method, and later the method was further extended by Cui *et al.* [2009] embedding the smoothing strain technique in such a problem. Leitão [2001] also developed a meshless method for static analysis of the Kirchhoff plate bending problems. Liew *et al.* [2004] and Liew *et al.* [1997] proposed the moving least-squares differential quadrature method and introduced the differential cubature method, respectively. Meshless LBIE formulations for simply supported and clamped plates under dynamic loading is studied by Sladek *et al.* [2003] while

Simkins *et al.* [2004] employed the reproducing kernel element method in terms of globally compatible C^n $(n \geq 1)$ triangular hierarchy. Zhou *et al.* [2006] performed the free vibration of rectangular plates with continuously distributed spring-mass. Recently, Cui *et al.* [2010] proposed an attractive technique based on the incorporation of various smoothing techniques and radial point interpolation method to static and free vibration analysis of thin plates without rotations, degrees of freedom (DOFs), etc.

As mentioned earlier, the paper addresses an alternative approach for constructing the shape functions; the moving Kriging (MK) interpolation is employed which [Gu, 2003] is pioneered. In fact, MK is a well-known geostatic technique for spatial interpolation in geology and mining but its application in mesh-free methods to structural problems is still young and potential. Gu [2003] successfully demonstrated the applicability of the MK interpolation solving a simple problem of steady-state heat conduction. Dai *et al.* [2003] then made a comparative study between the radial point and the Kriging interpolations for elasticity. A novel approach — Local Kriging (LoKriging) method is introduced by Lam *et al.* [2004] for two-dimensional cases, where the local weak form of the partial differential governing equations is used. Li *et al.* [2004] had further extended the LoKriging method for dynamic analysis of structures. Furthermore, some other investigations of the present method to solid mechanics and shell structures are examined by Tongsuk and Kanok-Nukulchai [2004a,b], and Sayakoummane and Kanok-Nukulchai [2007], respectively. Recently, Nguyen [2007] also successfully applied the MK-based mesh-free method to numerical simulation of classical thin plates.

The objective of the current work is to further develop the MK-based mesh-free method for other problems, and here for eigenvalue analysis of the thin plate structures with different complicated geometric shapes. Several numerical examples are considered in detail. Based on the best knowledge of the authors, no such task has been analyzed once this work is being reported.

2. Mesh-Free Moving Kriging Interpolation Method for Free Vibration

2.1. *MK shape functions construction*

In this section, the MK interpolation used for constructing the shape functions and their derivatives is briefly presented. For detailed description of other features one can refer to Gu [2003], Bui *et al.* [2009], and Tongsuk *et al.* [2004a,b]. Basically, the idea of the MK method is similar to that of the MLS, it is to approximate distribution functions $\mathbf{u}(\mathbf{x}_i)$ in a subdomain Ω_x, so that $\Omega_x \subseteq \Omega$. It also implies that these values can be interpolated based on all nodal values $\mathbf{x}_i$ $(i \in [1, n])$, with n the total number of the nodes in Ω_x. The MK interpolation $\mathbf{u}^h(\mathbf{x})$, $\forall\, \mathbf{x} \in \Omega_x$ is defined as

$$\mathbf{u}^h(\mathbf{x}) = [\mathbf{p}^{\mathrm{T}}(\mathbf{x})\mathbf{A} + \mathbf{r}^{\mathrm{T}}(\mathbf{x})\mathbf{B}]\mathbf{u}(\mathbf{x}) \tag{2.1}$$

or

$$\mathbf{u}^h(\mathbf{x}) = \sum_I^n \phi_I(\mathbf{x}) u_I \tag{2.2}$$

with $\phi_I(\mathbf{x})$ being the MK shape functions and defined by

$$\phi_I(\mathbf{x}) = \sum_j^m p_j(\mathbf{x}) A_{jI} + \sum_k^n r_k(\mathbf{x}) B_{kI}. \tag{2.3}$$

The matrices $\mathbf{A}$ and $\mathbf{B}$ given in Eq. (2.1) are determined by

$$\mathbf{A} = (\mathbf{P}^{\mathrm{T}}\mathbf{R}^{-1}\mathbf{P})^{-1}\mathbf{P}^{\mathrm{T}}\mathbf{R}^{-1} \tag{2.4}$$

and

$$\mathbf{B} = \mathbf{R}^{-1}(\mathbf{I} - \mathbf{P}\mathbf{A}) \tag{2.5}$$

where $\mathbf{I}$ is a unit matrix and the vector $\mathbf{p}(\mathbf{x})$ is the polynomial with m basis functions

$$\mathbf{p}(\mathbf{x}) = \begin{Bmatrix} p_1(\mathbf{x}) & p_2(\mathbf{x}) & \cdots & p_m(\mathbf{x}) \end{Bmatrix}^{\mathrm{T}} \tag{2.6}$$

For more clarification, on the one side, the matrix $\mathbf{P}$ of size $n \times m$ is the collected values of the polynomial basis functions presented in Eq. (2.6) at the given set of nodes

$$\mathbf{P} = \begin{bmatrix} p_1(\mathbf{x}_1) & p_2(\mathbf{x}_1) & \cdots & p_m(\mathbf{x}_1) \\ \vdots & \vdots & \ddots & \vdots \\ p_1(\mathbf{x}_2) & p_2(\mathbf{x}_2) & \cdots & p_m(\mathbf{x}_2) \\ p_1(\mathbf{x}_n) & p_2(\mathbf{x}_n) & \cdots & p_m(\mathbf{x}_n) \end{bmatrix} \tag{2.7}$$

and $\mathbf{r}(\mathbf{x})$ in Eq. (2.1) is also given as

$$\mathbf{r}(\mathbf{x}) = \begin{Bmatrix} R(\mathbf{x}_1, \mathbf{x}) & R(\mathbf{x}_2, \mathbf{x}) & \cdots & R(\mathbf{x}_n, \mathbf{x}) \end{Bmatrix}^{\mathrm{T}} \tag{2.8}$$

In Eq. (2.8), $R(\mathbf{x}_i, \mathbf{x}_j)$ is defined as the correlation function between any pair of the n nodes $\mathbf{x}_i$ and $\mathbf{x}_j$; it is denoted as belonging to the covariance of the field value $u(\mathbf{x})$: $R(\mathbf{x}_i, \mathbf{x}_j) = \mathrm{cov}[u(\mathbf{x}_i)u(\mathbf{x}_j)]$ and $R(\mathbf{x}_i, \mathbf{x}) = \mathrm{cov}[u(\mathbf{x}_i)u(\mathbf{x})]$. There exist many functions which could be used as a correlation function [Gu, 2003]. However, a Gaussian function is simply and widely used. A correlation parameter θ is then introduced to best fit the model

$$R(\mathbf{x}_i, \mathbf{x}_j) = e^{-\theta r_{ij}^2} \tag{2.9}$$

where $r_{ij} = \|\mathbf{x}_i - \mathbf{x}_j\|$ and $\theta > 0$ is a correlation parameter. In this study, the quadratic basis function $\mathbf{p}^{\mathrm{T}}(\mathbf{x}) = [1 \quad x \quad y \quad x^2 \quad y^2 \quad xy]$ is adopted to be used in numerical implementations. In addition, the form of Gaussian exponential correlation functions is provided by Giunta and Watson [1998].

$$R(\mathbf{x}_i, \mathbf{x}_j) = \exp\left[-\sum_{k=1}^m \theta_k \|x_i - x_j\|^2\right] \tag{2.10}$$

In Eq. (2.10), the correlation parameter $\theta > 0$ is obtained by maximizing the following function:

$$\theta = \max\left(\frac{-n\ln(\eta^2) + \ln(|R|)}{2}\right) \tag{2.11}$$

where the covariance η within Eq. (2.11) is ignored in this study. The quality of MK is heavily influenced by the correlation parameter θ. This correlation factor is studied in more detail in numerical analysis section. In addition, matrix $\mathbf{R}[R(\mathbf{x}_i, \mathbf{x}_j)]_{n\times n}$ is also given in an explicit form

$$\mathbf{R}[R(\mathbf{x}_i, \mathbf{x}_j)] = \begin{bmatrix} 1 & R(\mathbf{x}_1, \mathbf{x}_2) & \cdots & R(\mathbf{x}_1, \mathbf{x}_n) \\ R(\mathbf{x}_2, \mathbf{x}_1) & 1 & \cdots & R(\mathbf{x}_2, \mathbf{x}_n) \\ \vdots & \vdots & \ddots & \vdots \\ R(\mathbf{x}_n, \mathbf{x}_1) & R(\mathbf{x}_n, \mathbf{x}_2) & \cdots & 1 \end{bmatrix} \tag{2.12}$$

With respect to Kirchhoff plate problems, apart from the requirement of the first-order derivatives, the second-order derivatives are also necessary to be formed. These partial derivatives can be easily obtained by the derivatives of Eq. (2.3) against x_i

$$\phi_{I,i}(\mathbf{x}) = \sum_{j}^{m} p_{j,i}(\mathbf{x}) A_{jI} + \sum_{k}^{n} r_{k,i}(\mathbf{x}) B_{kI} \tag{2.13}$$

$$\phi_{I,ii}(\mathbf{x}) = \sum_{j}^{m} p_{j,ii}(\mathbf{x}) A_{jI} + \sum_{k}^{n} r_{k,ii}(\mathbf{x}) B_{kI} \tag{2.14}$$

In addition, it would be interesting in seeing how the MK shape functions and their derivatives up to second order look like, and Fig. 1 is made for such purpose.

2.2. *Radius of influence domain*

One of the other important things in meshless methods is the concept of influence domain where an influence domain radius is assigned to determine the number of scattered nodes within an interpolated domain of interest. In fact, no exact rules can be totally determinable to all types of nodal distributions. As studied previously this issue has a significant effect on the solution. Therefore, it should be chosen somehow to ensure that the problems can be converged. They might also be found in such a similar manner [Liu, 2003]. Often, the following formula is used to compute the size of the support domain.

$$d_m = \alpha d_c \tag{2.15}$$

where d_c is a characteristic length relative to the nodal spacing close to the point of interest while α stands for a scaling factor.

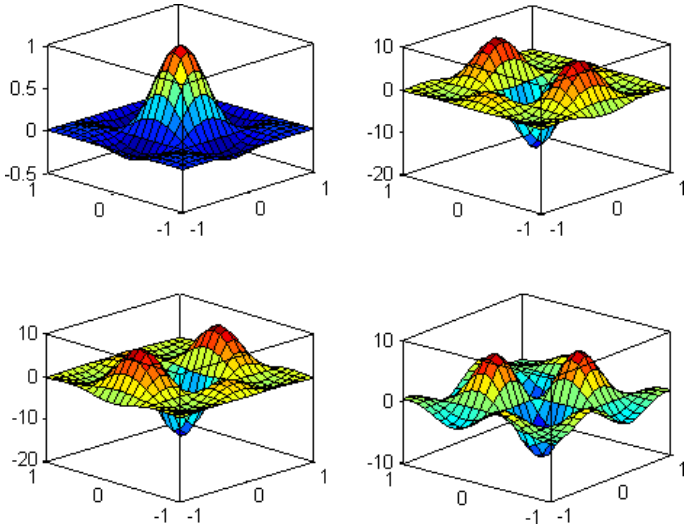

Fig. 1. The MK shape function (top-left) (a), second-order derivatives corresponding to xx-directions (top-right) (b), yy (bottom-left) (c), and xy (bottom-right) (d) with $\mathbf{p}^{\mathrm{T}}(\mathbf{x}) = [1 \quad x \quad y \quad x^2 \quad y^2 \quad xy]$.

2.3. *Effect of the correlation parameter on shape functions*

In this section, another important point concerning the influence of the correlation parameter given in Eq. (2.11) on the quality of the shape functions is briefly illustrated in two-dimensional setting. Normally, the accuracy of solutions is dependent on the quality of the shape functions. This is therefore evaluated by numerical investigations in the numerical part. The consideration of this issue in one dimension can also be found in the work by Bui *et al.* [2009] for detail. In the following, Fig. 2 shows a part of the MK shape functions at the corner with four different specified correlation parameters: 0.1, 20, 100, and 1000, respectively. It is evident that the smoothing feature of the shape functions is significantly affected by the correlation parameter. With $\theta = 0.1, 20$, the shape functions are smoother than the others, e.g., $\theta = 100, 1000$. Note that the choice of this parameter totally depends on the experience of analysts.

In practice, deriving optimal values of the correlation parameter for all problems is very difficult. It varies from one to another problem and in theory there are no exact rules to get such a single optimal value for all problems. Hence, it is of interest to alternatively evaluate the correlation parameter so that there should exist an acceptable range on its magnitude to ensure consistency in the quality of the results.

3. Discrete Governing Equation

The governing equations and discretization of the Kirchhoff thin plates are essentially presented in this section. Consider a plate of Ω under a Cartesian coordinate

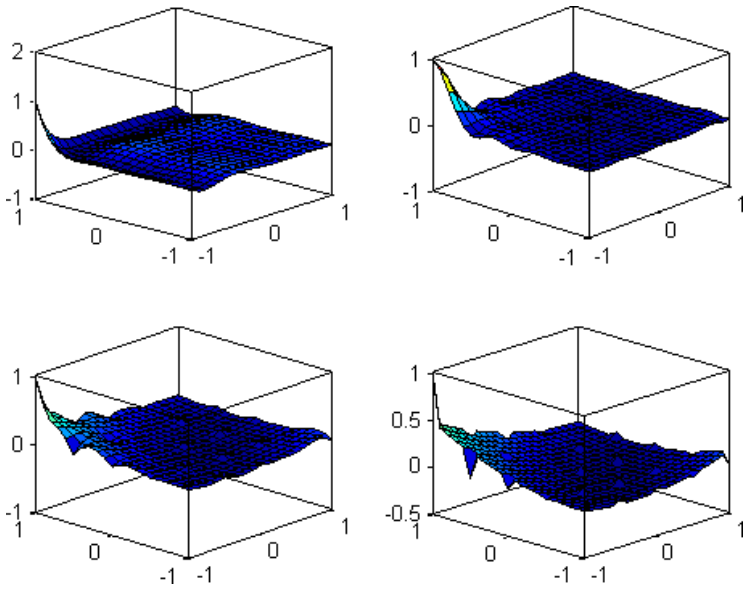

Fig. 2. Influence of the correlation parameter vs. the quality of MK shape function. $\theta = 0.1, 20, 100$, and 1000 correspond to the top-left, top-right, bottom-left, and bottom-right, respectively.

system; the deflections of the plate in the x-, y-, z-directions are denoted as u, v, w, respectively. The plate is represented by a set of scattered nodes in the problem domain of interest. The deflection $w(\mathbf{x})$ with $\mathbf{x} = \{x, y\}^{\mathrm{T}}$ is directly approximated using parameters of nodal deflection w_I expressed as

$$w^h(\mathbf{x}) = \sum_I^n \phi_I(\mathbf{x}) w_I \quad \text{with } \mathbf{x} \in \Omega \tag{3.1}$$

where the $\phi_I(\mathbf{x})$ are known as the mesh-free MK shape functions given in Eq. (2.3), where n is the number of scattered nodes in the support domain at the point of interest.

The dynamic equilibrium equation of a plate in a strong form for homogeneous and isotropic can be represented in a fourth-order equation as

$$D_t \nabla^4 w + \rho h \ddot{w} = q_z \tag{3.2}$$

where ρ and q_z denote the mass density of the materials and the lateral loading, respectively, and

$$D_t = \frac{Eh^3}{12(1-\nu^2)} \tag{3.3}$$

is the flexural rigidity, and E, ν, and h are the Young's modulus, the Poisson's ratio, and the thickness of the plate, respectively. The constitutive equations representing the relationship between the strains and stresses are generally expressed in terms

of the generalized Hooke's law [Liu, 2003; Liu and Chen, 2001] as

$$\boldsymbol{\sigma}_p = \mathbf{D}\boldsymbol{\varepsilon}_p \tag{3.4}$$

where $\mathbf{D}$ is the matrix of constants relative to the material property and the thickness of the plate, $\boldsymbol{\sigma}_p$ and $\boldsymbol{\varepsilon}_p$ are defined as pseudostrains and pseudostresses. For homogeneous plate, they simply have

$$\mathbf{D} = D_t \begin{bmatrix} 1 & \nu & 0 \\ \nu & 1 & 0 \\ 0 & 0 & (1-\nu)/2 \end{bmatrix} \tag{3.5}$$

$$\boldsymbol{\varepsilon}_p = \left\{ -\frac{\partial^2 w}{\partial x^2} \quad -\frac{\partial^2 w}{\partial y^2} \quad -2\frac{\partial^2 w}{\partial x \partial y} \right\}^{\mathrm{T}} = \mathbf{L}w \tag{3.6}$$

$$\boldsymbol{\sigma}_p = \left\{ M_x \quad M_y \quad M_{xy} \right\}^{\mathrm{T}} \tag{3.7}$$

In Eq. (3.7), M_x, M_y, and M_{xy} are components of bending moments and twisting moment, respectively. By means of the Kirchhoff's plates assumption, the deflection $w(\mathbf{x})$ can be independently variable, whereas the other two displacement components $u(\mathbf{x})$ and $v(\mathbf{x})$ can be extracted from $w(\mathbf{x})$. The displacement fields of the Kirchhoff plate also have

$$\mathbf{u} = \{u \quad v \quad w\}^{\mathrm{T}} = \left\{ -z\frac{\partial w}{\partial x} \quad -z\frac{\partial w}{\partial y} \quad w \right\}^{\mathrm{T}} = \hat{\mathbf{L}}^{\mathrm{T}} w \tag{3.8}$$

For free vibration analysis, the weak Galerkin form of the elastodynamic undamped equilibrium equation can be written as [Liu, 2003]

$$\int_\Omega \delta\boldsymbol{\varepsilon}_p^{\mathrm{T}} \boldsymbol{\sigma}_p d\Omega + \int_\Omega \delta\mathbf{u}^{\mathrm{T}} \rho \ddot{\mathbf{u}} d\Omega = 0 \tag{3.9}$$

It is noted that free external forces are taken into account for the free vibration analysis of the plate. The dynamic variational form Eq. (3.9) can be rewritten as

$$\int_\Omega \delta(\mathbf{L}w)^{\mathrm{T}} \mathbf{D}(\mathbf{L}w) d\Omega + \int_\Omega \delta(\hat{\mathbf{L}}w)^{\mathrm{T}} \rho \hat{\mathbf{L}} \ddot{w} d\Omega = 0 \tag{3.10}$$

Substituting the deflection field w in Eq. (3.1) into the variational form shown in Eq. (3.10), the final undamped dynamic discrete equation for free vibration analysis is obtained as follows

$$\mathbf{M}\ddot{\mathbf{w}} + \mathbf{K}\mathbf{w} = 0 \tag{3.11}$$

where $\mathbf{w}, \mathbf{K}$, and $\mathbf{M}$ are the vectors of general nodal deflections, the global stiffness, and the mass matrices, respectively. They are

$$K_{IJ} = \int_\Omega \mathbf{B}_I^{\mathrm{T}} \mathbf{D} \mathbf{B}_J d\Omega \tag{3.12}$$

$$M_{IJ} = \int_{\Omega} (\rho \phi_I \phi_J h + \phi_{I,x} \phi_{J,x} I + \phi_{I,y} \phi_{J,y} I) d\Omega \tag{3.13}$$

$$\mathbf{B}_I = \begin{Bmatrix} -\phi_{I,xx} & -\phi_{I,yy} & -2\phi_{I,xy} \end{Bmatrix}^{\mathrm{T}} \tag{3.14}$$

where $I = \rho(h^3/12)$ is the mass moment of inertia for the homogeneous plate. It is noteworthy that the first team of Eq. (3.13) is the mass inertia corresponding to the vertical translational vibration. In the case where the thickness of the plate is too small, a very thin plate, the other two teams in the mass matrix standing for rotational inertia corresponding to the rotational vibration can be neglected [Liu, 2003]. As a consequence, a general solution of such a homogeneous equation can be written as

$$\mathbf{w} = \bar{\mathbf{w}} e^{i\omega t} \tag{3.15}$$

where i is the imaginary unit, t indicates time, $\bar{\mathbf{w}}$ is the eigenvector, and ω is natural frequency. Inserting Eq. (3.15) into Eq. (3.11), the natural frequency ω of the plates can be found by solving the following eigenvalue equation:

$$(\mathbf{K} - \omega^2 \mathbf{M}) \bar{\mathbf{w}} = 0 \tag{3.16}$$

The orthogonal transformation technique presented by Liu and Chen [2001] is also used to implement the essential boundary condition in the eigenvalue equation. From here, it can be easily seen that the obtained present formulations for free vibration analysis of thin plates are simple and similar as the traditional FEM.

4. Numerical Results

The applicability of the proposed method is illustrated by solving various examples of thin plates with different geometries of complicated shapes. The accuracy of the results is very important compared with other numerical approaches and the analytical solutions available in the literature. Four examples are taken into account including a square, a L-shape, a square plate with a complicated hole, and a square plate with four closed holes subjected to the completely free and simply supported boundary conditions. The influence of the scaling factor and the correlation parameter on natural frequencies is also considered.

Only the completely free and the simply supported boundaries are considered throughout the paper, whereas the clamped boundary is not available due to the lack of deflection derivatives in the interpolation functions. The deflection derivatives, i.e., two rotations, must be defined as unknown variables in the interpolation functions. However, these derivatives cannot be imposed directly because no information of such derivatives is involved in the MK approximation functions given in Eq. (2.1). Nevertheless, one possible strategy has been suggested by Liu *et al.* [2006] and Cui *et al.* [2009] by introducing an efficient Hermite-type technique embedded in the RPIM, where both deflection and its derivatives are defined as field variables in the interpolation functions. The other strategy is based on the recent work of Cui

et al. [2010] who introduced a very interesting study of a development incorporated between various types of smoothing techniques and the radial point interpolation method. The present MK technique might use a similar remedy but it demands a development evidently. However, all these tasks are in general more challenging and beyond the scope of the present work.

4.1. *Square plate*

As seen above the present work is mainly concentrated on free vibration analysis of plates with complicated shapes. For completeness, a thin square plate is considered as the first numerical example with the following parameters: $a = b = 10\,\mathrm{m}$, the thickness $h = 0.01\,\mathrm{m}$, Young's modulus $E = 2 \times 10^{11}\,\mathrm{N/m^2}$, Poisson's ratio $\nu = 0.3$, and the mass density $\rho = 8000\,\mathrm{kg/m^3}$ [Cui *et al.*, 2010]. The frequencies are calculated by the present method for both regular and irregular distributions of 289 nodes subjected to the completely free and the simply supported boundaries. For all the computations, a background cell of 16 Gaussian points is chosen for the purpose of numerical integrations. A scaling factor of 2.8 interpreting the size of the support and a correlation parameter of 5 are used. The natural frequency coefficient (NFC) defined as $\Omega_1 = (\omega^2 \rho h a^4/D_t)^{1/4}$ is used. The results of the completely free and the simply supported boundaries are presented in Tables 1 and 2, respectively. In Table 1, the first three frequencies corresponding to rigid displacements are zero and not listed in the table. In Table 2, the first ten frequencies are presented. All the results are compared with the analytical solutions [Abbassian *et al.*, 1987] and the RPIM based on smoothed techniques [Cui *et al.*, 2010]. As a result, a very good agreement for both the completely free and the simply supported boundaries is obtained.

4.2. *L-shape plate*

4.2.1. *Free boundary condition*

The second example deals with a L-shape thin plate whose geometric parameters are depicted in Fig. 3. A scaling factor of 2.5 and a correlation parameter of 20 are

Table 1. A comparison of the NFCs of the completely free square plate among the present, the smoothed-RPIM methods, and the exact solutions.

Mode	Exact	NS-RPIM	ES-RPIM	CS-RPIM	Present: 289 nodes	
					Regular	Irregular
4	3.670	3.667	3.671	3.667	3.671	3.679
5	4.427	4.396	4.405	4.414	4.421	4.436
6	4.926	4.914	4.911	4.916	4.930	4.938
7	5.929	5.883	5.875	5.877	5.927	5.962
8	5.929	5.898	5.894	5.892	5.927	5.962
9	7.848	7.761	7.762	7.780	7.862	7.923

Note: The first three frequencies corresponding to rigid displacements are not listed.

Table 2. A comparison of the NFCs of the simply supported square plate among the present, the smoothed-RPIM methods, and the exact solutions.

Mode	Exact	NS-RPIM	ES-RPIM	CS-RPIM	Present: 289 nodes	
					Regular	Irregular
1	4.443	4.439	4.443	4.443	4.444	4.469
2	7.025	7.003	7.020	7.026	7.026	7.154
3	7.025	7.008	7.025	7.029	7.026	7.154
4	8.886	8.861	8.880	8.884	8.895	8.946
5	9.935	9.887	9.930	9.948	9.923	9.955
6	9.935	9.890	9.930	9.949	9.924	9.982
7	11.327	11.264	11.308	11.323	11.313	11.381
8	11.327	11.287	11.322	11.335	11.315	11.911
9	12.953	12.867	12.951	12.984	12.933	12.977
10	12.953	12.869	12.951	12.985	12.949	13.018

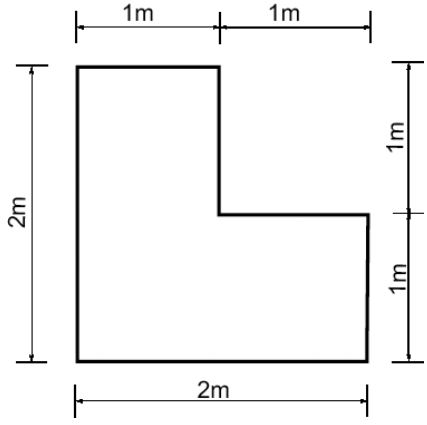

Fig. 3. The geometric parameters of the thin L-shape plate.

indicated in the computation. Both regular and irregular distributions of nodes are taken and two patterns of 121 and 289 nodes are shown in Fig. 4. The thickness $h = 0.05\,\mathrm{m}$ is taken and other material parameters are the same as the square plate. Because no exact solution for this problem is available, an extra solution performed through the standard EFG is implemented as assumed to be a reference one. The implemented results obtained of both methods are listed in Table 3, in which the first three frequencies corresponding to rigid displacements were not listed. A good agreement between the EFG and the proposed methods can be found accordingly.

An investigation of the influence of the scaling factor and the correlation parameter on the frequencies is also examined and their computed NFCs results are presented in Tables 4 and 5, respectively. As it can be observed from the achieved results, the acceptable solutions can be obtained with a value of $2 \leq \alpha \leq 4$ for the scaling factor and a value of $1 \leq \theta \leq 100$ for the correlation parameter. While, with $\alpha = 6$, which probably affects on the amount of scattered nodes inside the

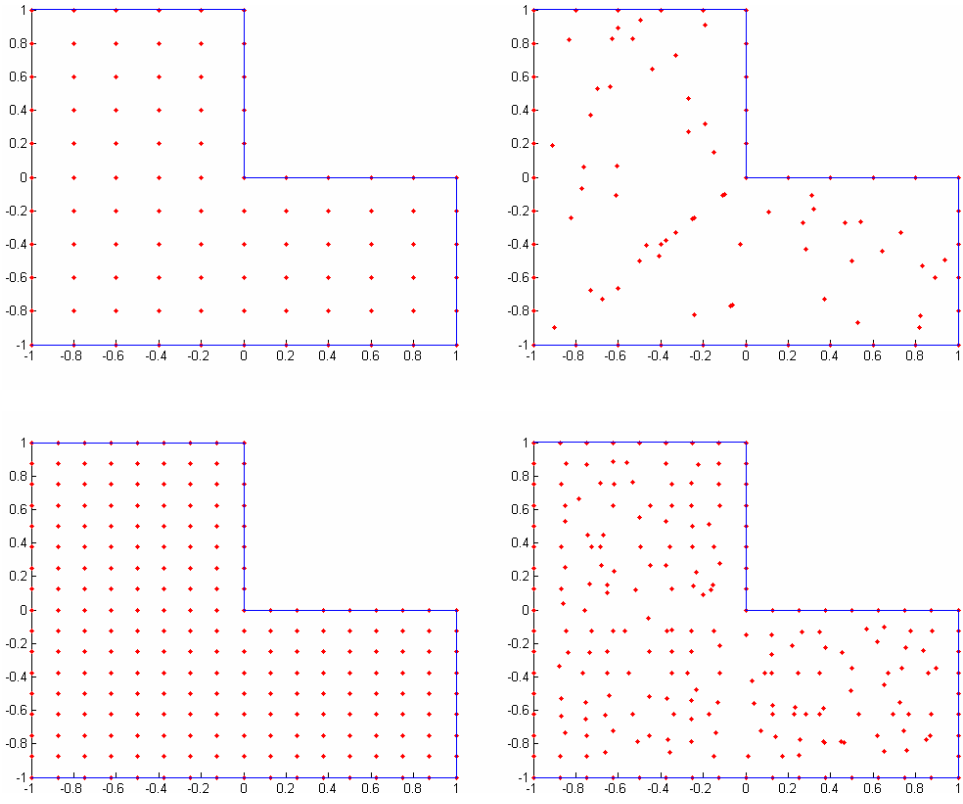

Fig. 4. Nodal distributions in the plate with regular and irregular nodal distributions: 121 (top) and 289 (bottom).

Table 3. A comparison of the NFCs of the free L-shape plate between the standard EFG and the present methods.

Mode	EFG	Present method		EFG	Present method	
	Regular 121 nodes	Regular 121 nodes	Irregular 121 nodes	Regular 289 nodes	Regular 289 nodes	Irregular 289 nodes
4	4.0221	4.0456	3.9686	3.9796	3.9694	3.9367
5	4.1987	4.2152	4.2076	4.1790	4.1284	4.1375
6	5.2698	5.2752	5.1796	5.2253	5.2122	5.1946
7	5.8585	5.7393	5.7176	5.8294	5.7109	5.6955
8	7.9138	7.7085	7.5818	7.7726	7.6153	7.5736
9	7.9171	7.9748	7.9090	7.8009	7.7838	7.7563
10	8.1853	8.3407	8.2354	8.0450	8.1233	8.0955

Note: The first three frequencies corresponding to rigid displacements are not listed.

influence domain which leads to an expensive computation and a certain influence to the interpolation, a higher error can be seen in this case. It is also found that the error is increased once $\theta > 100$. Figure 5 presents the first 20 eigenmodes of the L-shape plate computed by the present method.

Table 4. The variation of NFCs vs. the scaling factor α of free thin L-shape plate compared to EFG.

Mode	EFG 289 nodes	Proposed method				
		$\alpha = 2.0$	$\alpha = 2.5$	$\alpha = 3.0$	$\alpha = 4.0$	$\alpha = 6.0$
4	3.9796	3.9647	3.9694	3.9566	3.9684	4.1616
5	4.1790	4.1189	4.1284	4.1300	4.0911	4.5680
6	5.2253	5.1950	5.2122	5.1958	5.1683	5.9701
7	5.8294	5.7497	5.7109	5.6487	5.6135	6.3310
8	7.7726	7.6444	7.6153	7.4568	7.3882	8.1275
9	7.8009	7.6944	7.7838	7.7672	7.5839	8.5850
10	8.0450	7.9518	8.1233	8.1239	7.9841	9.0283

Note: The correlation coefficient $\theta = 20$ is fixed.

Table 5. The influence of the correlation parameter θ on the natural frequency of free L-shape plate.

Mode	EFG 289 nodes	Proposed method					
		$\theta = 1$	$\theta = 5$	$\theta = 20$	$\theta = 100$	$\theta = 300$	$\theta = 1000$
4	3.9796	3.4265	3.9116	3.9694	4.0030	4.5462	4.8670
5	4.1790	4.0544	4.1015	4.1284	4.1384	4.9859	5.1912
6	5.2253	4.7954	5.1335	5.2122	5.2361	5.7817	6.2718
7	5.8294	4.9047	5.4999	5.7109	5.7564	6.7666	6.9264
8	7.7726	5.8793	7.0423	7.6153	7.7868	8.6528	8.8990
9	7.8009	7.6907	7.6762	7.7838	7.7870	9.0452	9.2715
10	8.0450	8.0295	8.0200	8.1233	8.1093	9.7615	9.8971

Note: The scaling factor $\alpha = 2.8$ is specified.

4.2.2. *Simply supported boundary condition*

The simply supported boundary for the thin L-shape plate is now considered. The problem is performed in the same manner as the free one above but the simply supported boundary condition is taken instead. The computed results gained by the MK-based mesh-free method are presented in Table 6, in which a comparison of the NFCs to that of the standard EFG for both regular and irregular nodal systems is given. The first six eigenmodes of the plate are provided in Fig. 6, and the influence of the scaling and the correlation coefficients on frequencies are presented in Tables 7 and 8, respectively. Figure 7 shows the results of the effect of the correlation parameter on the natural frequencies. A good agreement between the two methods is found. The same conclusion for the scaling and the correlation parameters given in the previous example is obtained. This implies that $2 \leq \alpha \leq 4$ and $1 \leq \theta \leq 100$ should be chosen in practice so that the method can give a good solution; otherwise a high error is encountered.

4.3. *Thin plate with a complicated shaped hole*

A thin plate with a hole of complicated shape is considered as the next numerical example in this section. The geometric relevant parameters found in the studies of

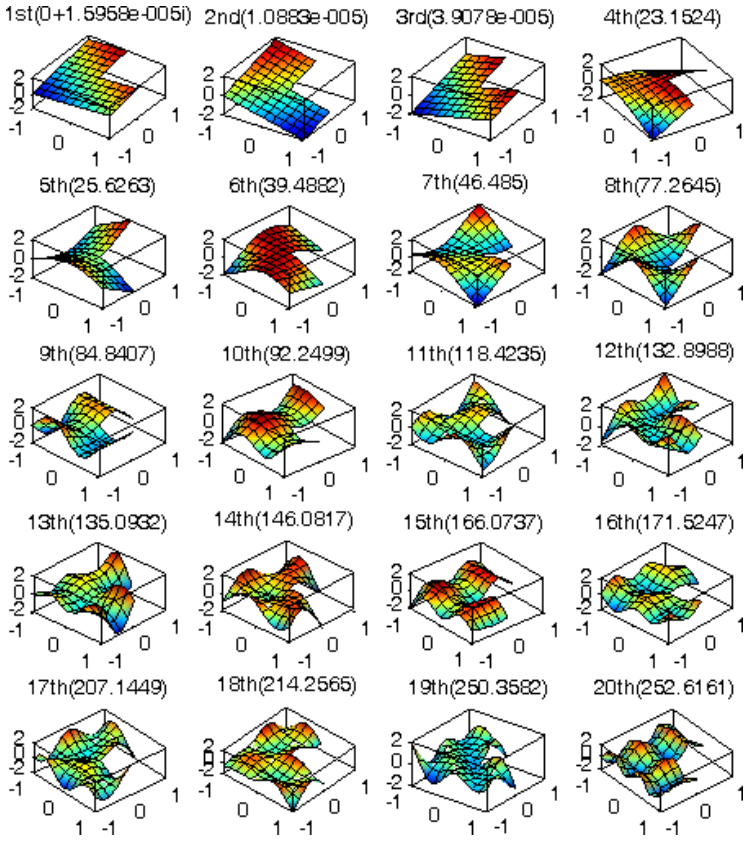

Fig. 5. The first 20 eigenmodes of the free L-shape plate computed by the present method.

Table 6. A comparison of the NFCs of the simply supported L-shape plate between the standard EFG and the present methods ($\alpha = 2.7$; $\theta = 5$).

Mode	EFG	Present 121 nodes		EFG	Present 289 nodes	
	Regular	Regular	Irregular	Regular	Regular	Irregular
1	6.7607	6.9326	6.9392	6.7649	6.8204	6.8040
2	8.2725	7.7894	7.8957	8.0319	7.9560	7.9417
3	8.9095	8.4547	8.6027	8.8821	8.4489	8.4342
4	10.9712	10.8628	10.8276	10.8853	10.4509	10.4768
5	11.5757	11.7246	11.6174	11.5584	11.1064	11.1182
6	13.1187	13.7591	13.3853	13.0156	13.2219	13.0766
7	14.1088	14.1065	13.8371	13.7309	13.3820	13.2651
8	14.2289	14.4653	14.0787	14.0279	13.9626	13.9128
9	14.4581	14.4930	14.4142	14.0442	14.0655	14.0117
10	15.5902	15.5424	15.2822	15.1630	15.2255	15.2521

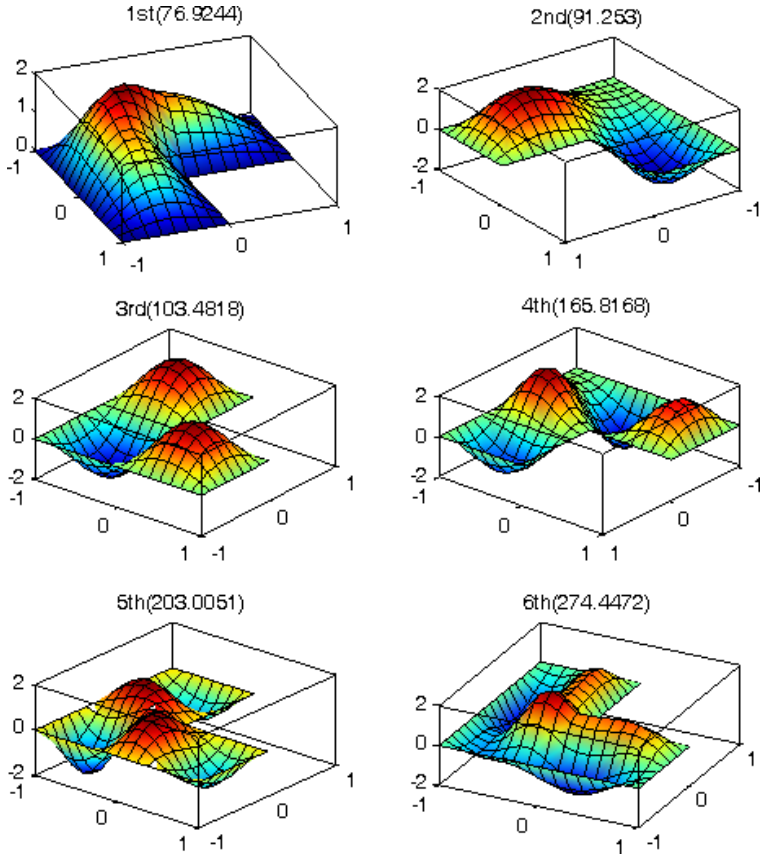

Fig. 6. The first six eigenmodes of the simply supported L-shape plate computed by the present method.

Table 7. The variation of the NFCs Ω_1 vs. the scale factor α of the simply supported thin square plate compared to the EFG.

Mode	EFG 289 nodes	$\alpha = 2.0$	$\alpha = 2.5$	$\alpha = 3.0$	$\alpha = 4.0$	$\alpha = 6.0$
1	6.7649	6.8624	6.9804	6.8970	6.8366	7.1091
2	8.0319	7.6931	7.6560	7.5724	7.5462	7.8038
3	8.8821	8.6780	8.4089	8.1664	8.2053	9.0604
4	10.8853	10.5660	10.4509	10.2241	10.2691	11.1771
5	11.5584	11.2836	11.1064	10.7933	11.1870	12.2067
6	13.0156	12.7517	13.2219	13.2027	12.7896	13.9051
7	13.7309	13.0121	13.3820	13.3066	13.1278	14.5426
8	14.0279	13.5061	13.5626	13.3517	13.5406	15.1431
9	14.0442	13.5089	13.5655	13.4204	13.5542	15.8912
10	15.1630	14.5118	14.3255	14.0200	14.9677	16.5266

Note: The correlation coefficient $\theta = 20$ is fixed.

Table 8. Variation of natural frequency coefficients vs. the correlation parameters of the simply supported thin L-shape plate.

Mode	EFG 169 nodes	Proposed method					
		$\theta = 1$	$\theta = 5$	$\theta = 20$	$\theta = 100$	$\theta = 300$	$\theta = 1000$
1	6.765	7.594	6.905	6.987	7.183	7.789	8.892
2	8.262	8.245	7.522	7.694	8.100	8.962	10.367
3	8.913	8.608	8.062	8.353	9.027	10.517	12.567
4	11.047	12.219	10.267	10.625	11.325	12.907	15.579
5	11.669	14.386	11.111	11.360	12.309	14.444	17.703
6	13.266	15.445	13.215	13.553	14.031	15.351	18.850
7	14.238	16.360	13.481	13.794	14.511	16.111	19.900
8	14.321	18.705	13.796	14.067	15.020	17.610	22.091
9	14.347	18.971	13.808	14.097	15.052	17.681	22.360
10	15.343	22.010	15.056	14.983	16.341	20.355	26.515

Note: The scaling factor $\alpha = 2.8$ is indicated.

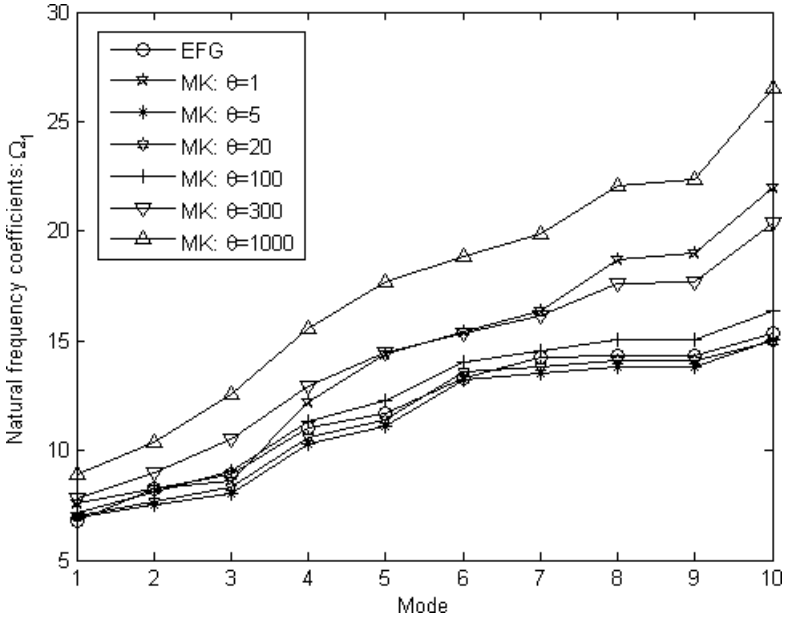

Fig. 7. Variation of the NFCs vs. the correlation parameter θ of the simply supported thin L-shape plate.

Liu [2003] and Liu and Chen [2001] are employed. Two distributions of 134 and 506 nodes are given in Fig. 8. Other parameters concerning the materials are the same as the L-shape plate. A scaling factor of 3.0 and a correlation parameter of 40 are specified in the implementation. Similarly, we calculate the NFCs Ω_1, and the results for the completely free boundary conditions are presented in Tables 9 and 10 considering two important parameters θ and α, respectively. The first six eigenmodes of the free boundary condition is plotted in Fig. 9. It is noted that

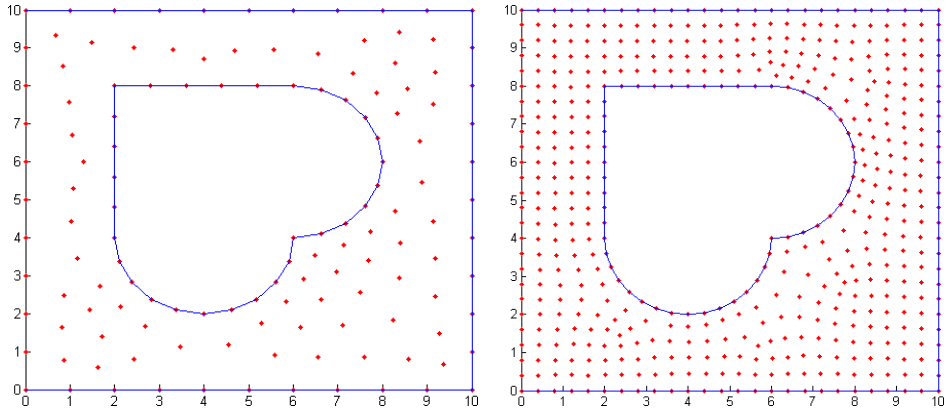

Fig. 8. Nodal distribution in the plate with a complicated shape hole: 134 nodes (left) and 506 nodes (right).

Table 9. Variation of the NFCs vs. the correlation parameters θ of the completely free thin plate with a hole of complicated shape.

Mode	Present method					
	$\theta = 1$	$\theta = 5$	$\theta = 20$	$\theta = 100$	$\theta = 300$	$\theta = 500$
4	3.3260	3.3673	3.3935	3.3611	3.2673	3.0739
5	3.8577	4.0450	4.2488	4.1978	3.8586	3.5723
6	4.8282	5.4967	5.9120	5.8246	4.8038	4.3518
7	5.4868	6.1095	7.3990	7.3216	5.6005	5.0498
8	5.5526	6.1952	7.7121	7.5118	5.6496	4.9870
9	7.2031	8.2838	9.1309	8.8514	7.2605	6.8500
10	7.7305	9.0642	9.7893	9.4577	7.7695	7.0581

Note: The scaling factor $\alpha = 3.0$ is taken.

Table 10. The variation of NFCs Ω_1 vs. the scale factor α of the completely free thin plate with a complicated shape hole.

Mode	Present method				
	$\alpha = 2.0$	$\alpha = 2.5$	$\alpha = 3.0$	$\alpha = 4.0$	$\alpha = 6.0$
4	3.3131	3.3583	3.3931	3.4734	4.2910
5	3.9969	4.1419	4.2773	4.3816	5.0821
6	5.3207	5.7263	5.9362	6.0500	6.9711
7	5.9603	6.5888	7.6390	10.7430	11.8624
8	5.9905	6.7516	8.0050	11.2122	12.0092
9	8.0102	8.6230	9.2254	12.6081	14.1772
10	8.5670	9.3449	9.8929	13.3977	17.5241

Note: The correlation coefficient $\theta = 40$ was fixed.

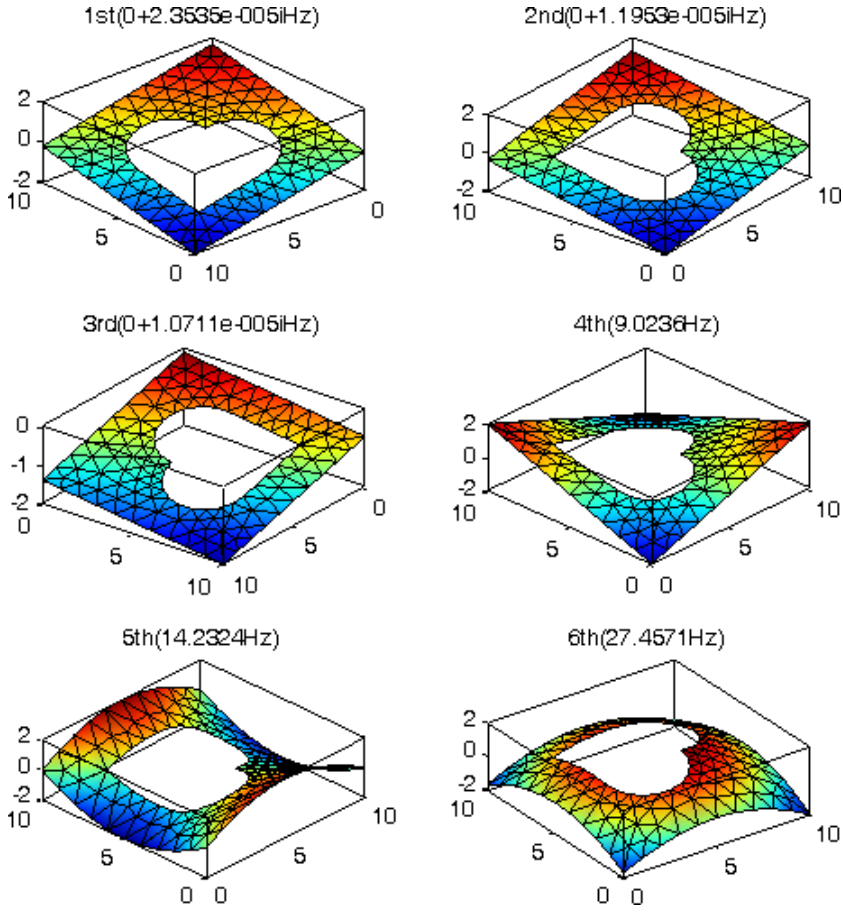

Fig. 9. The first six eigenmodes of the free thin plate with a complicated hole obtained by the proposed method.

the first three frequencies corresponding to the rigid displacements are not listed in the tables. In Fig. 9, these rigid displacements are also involved to illustrate the accurate implementation of the proposed method.

For the simply supported boundary condition, the results correspondingly obtained by the present method are presented in Table 11 and Fig. 10, in which a comparison with the result studied by Liu and Chen [2001] for the case of S-S-S-S boundary condition is found. A good agreement is observed evidently. The first 20 eigenmodes is also presented in Fig. 11.

4.4. *Thin plate with four holes*

The last numerical example examining a thin plate with four holes as depicted in Fig. 12 including its nodal distributions 131 and 457, respectively, is considered. The material parameters are the same as the L-shape plate. As above, the completely

Table 11. A comparison of natural frequency coefficients Ω_1 of the simply supported thin plate with a complicated hole between the EFG and the present methods ($\alpha = 3$; $\theta = 40$).

Mode	Liu and Chen [2001] S-S-S-S	Present method	
		134 nodes	506 nodes
1	5.453	5.3647	5.3898
2	8.069	7.4907	7.5023
3	9.554	8.0340	8.3470
4	10.099	10.2125	10.6358
5	11.328	10.9203	11.0484
6	12.765	12.7610	12.8945
7	13.685	12.8975	13.7100
8	14.305	13.6332	14.0620
9	15.721	15.5574	16.6492
10	17.079	16.2277	17.3641

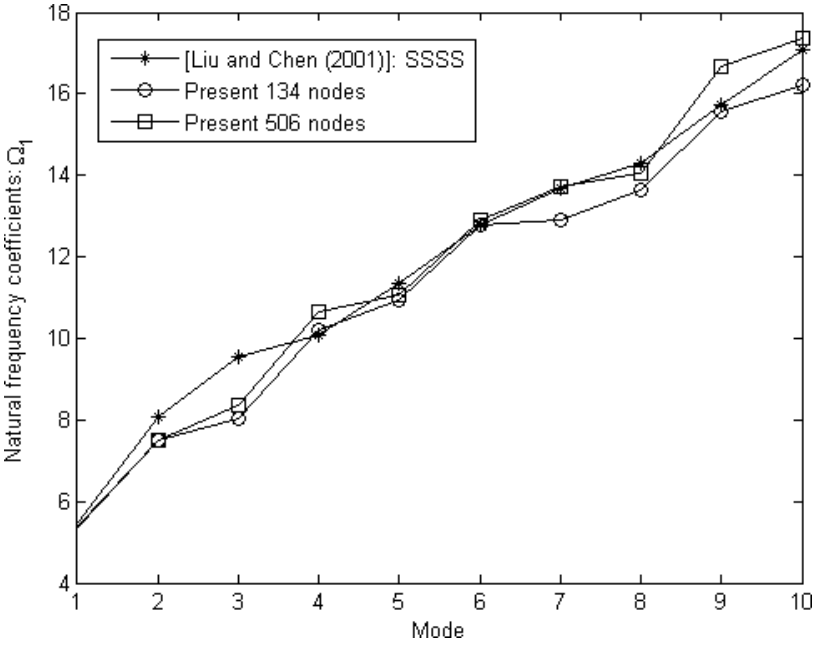

Fig. 10. Comparison of the NFCs of the simply supported thin plate with a complicated shape hole between the present method and the EFG studied by Liu and Chen [2001].

free and the simply supported boundary conditions are considered. Because no exact solutions are available for this configuration example, an appropriate solution based on the FEM (ANSYS) with a very fine mesh (95355 degrees-of-freedom — DOFs) as a reference solution, is assumed to be as close as a pseudo-analytical solution. Tables 12 and 13 show the results of natural frequencies implemented by the FEM and the present method, respectively. A very good agreement is obtained.

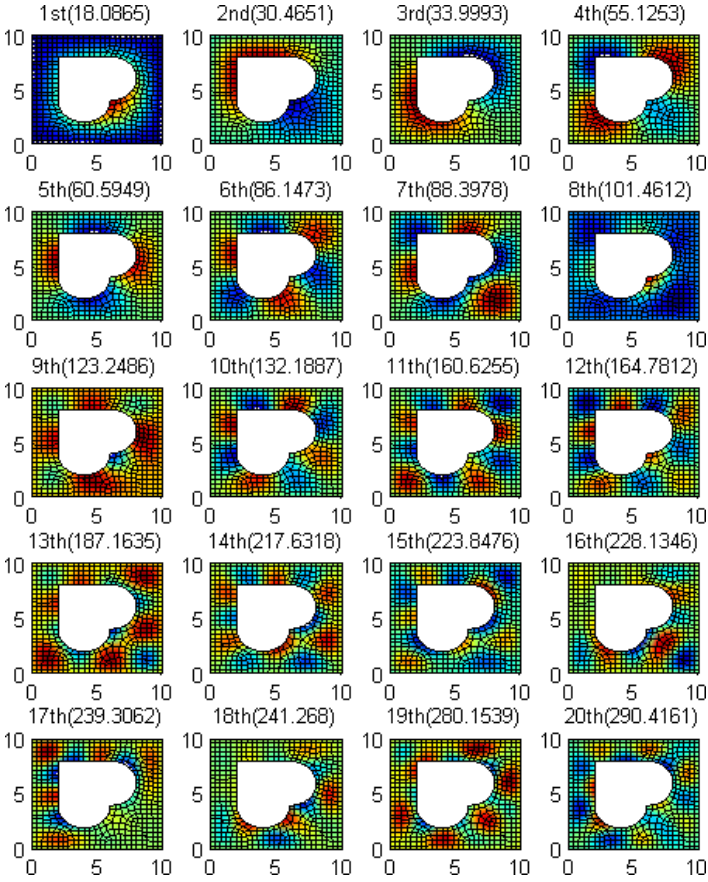

Fig. 11. The first 20 eigenmodes of the simply supported thin plate with a complicated shape hole obtained by the proposed method.

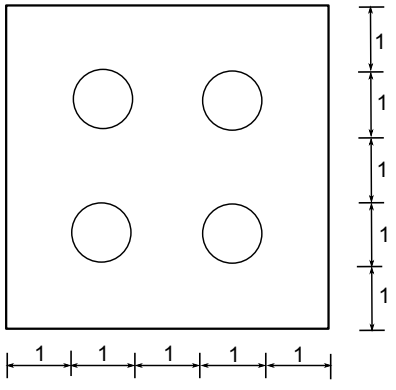

(a)

Fig. 12. The geometry (a) and nodal distributions of the plate with four circular holes of 131 (b) and 457 (c) scattered nodes.

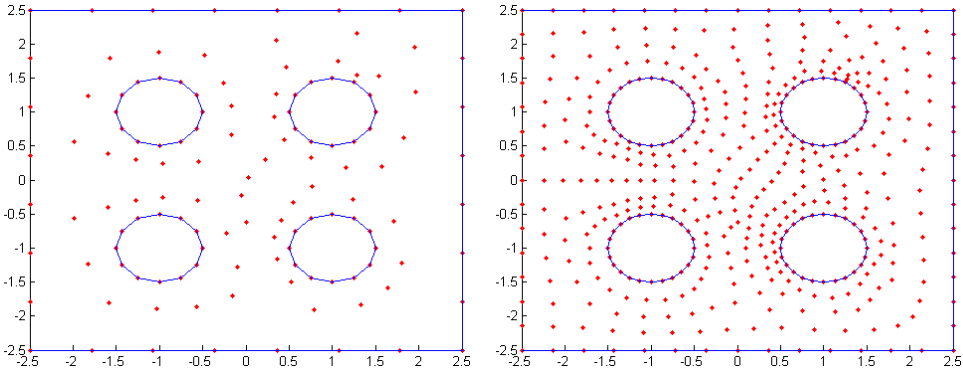

(b) (c)

Fig. 12. (*Continued*)

Table 12. A comparison of natural frequency of free thin plate with four holes between the FEM and the present method ($\alpha = 2.7$; $\theta = 3.0$).

Mode	FEM (ANSYS 95355 DOFs[a])	Present method	
		131 nodes	457 nodes
4	30.319	32.063	29.916
5	43.119	45.878	43.110
6	50.468	54.854	50.450
7	78.583	72.673	75.550
8	78.583	72.959	75.752
9	133.944	142.686	129.065
10	133.951	148.123	134.401

[a]DOFs: Degrees of freedom. The first three modes corresponding to the rigid displacements are not listed.

Table 13. A comparison of natural frequency of simply supported thin plate with four holes between the FEM and the present method ($\alpha = 2.7$; $\theta = 3.0$).

Mode	FEM (ANSYS 95355 DOFs)	Present method	
		131 nodes	457 nodes
1	45.241	40.113	42.265
2	113.932	116.196	110.580
3	113.939	117.131	113.410
4	193.258	192.674	192.951
5	219.056	248.420	208.137
6	221.783	252.496	219.175
7	286.406	326.564	281.496
8	286.425	338.155	283.604
9	378.945	432.292	378.441
10	378.970	441.435	379.808

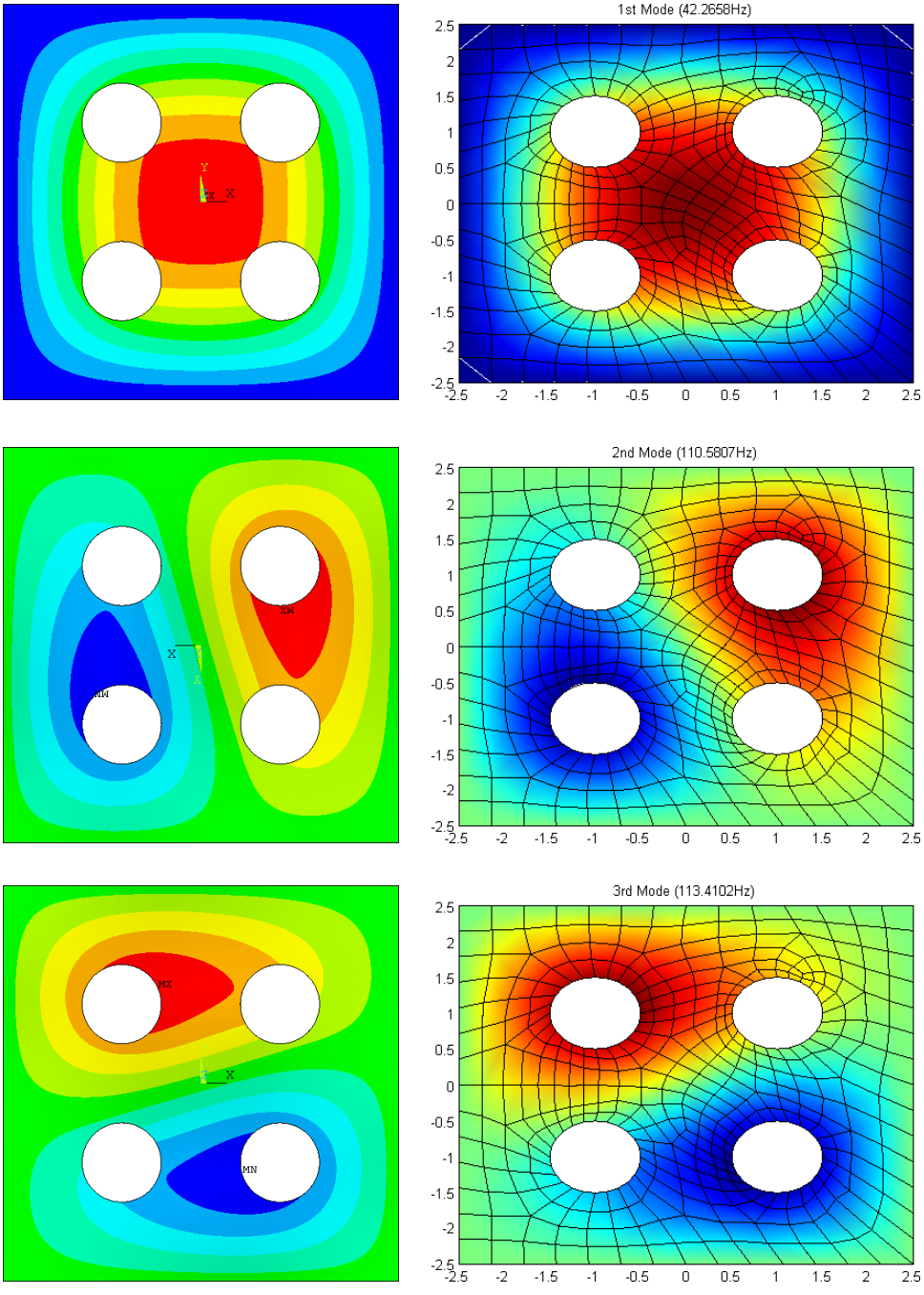

(a)

Fig. 13. (a) Comparison of the first six eigenmodes between the FEM (ANSYS) (left) and the present method (right): modes 1, 2, and 3, respectively.

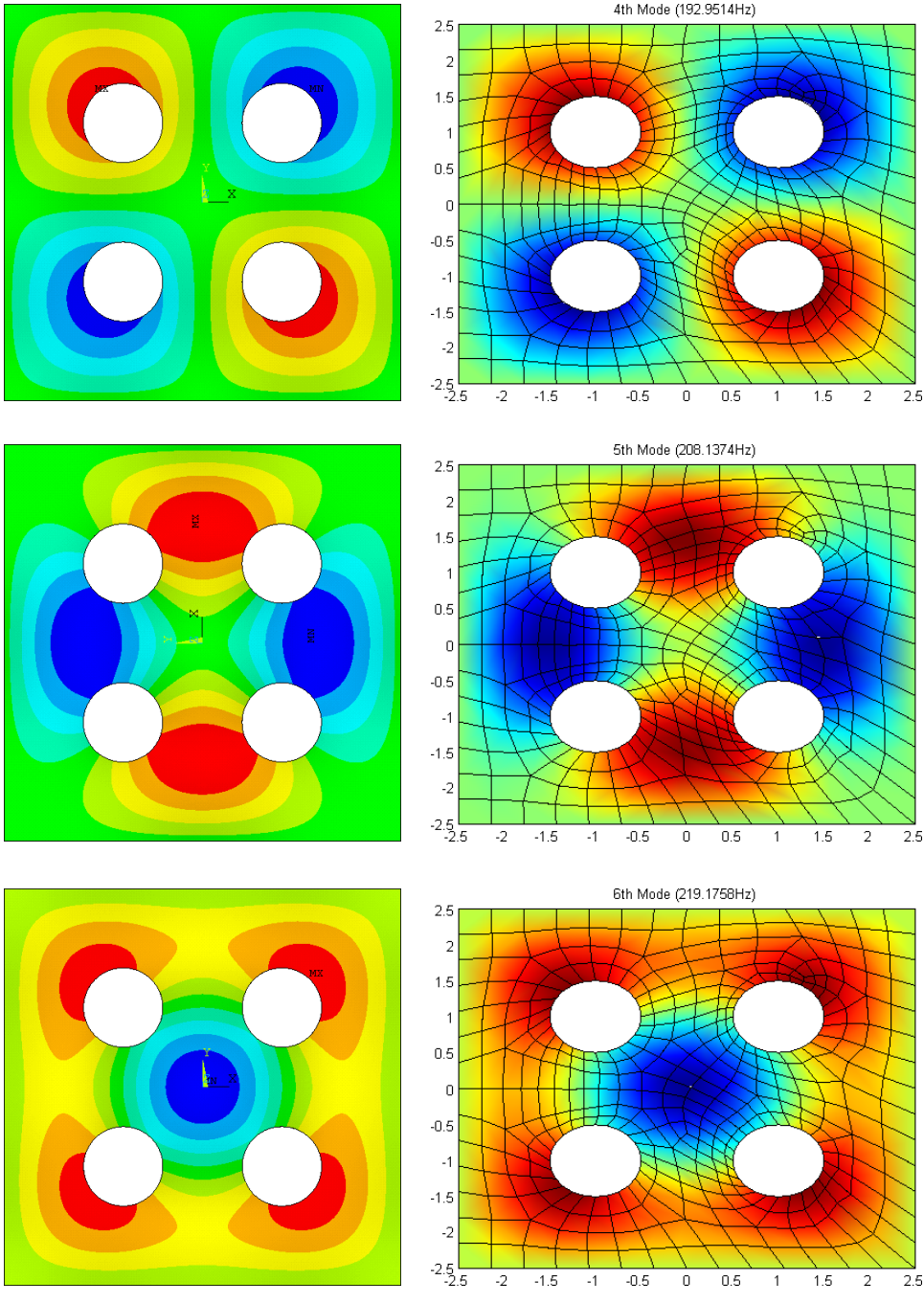

(b)

Fig. 13. (b) Comparison of the first six eigenmodes between the FEM (ANSYS) (left) and the present method (right): modes 4, 5, and 6, respectively.

Furthermore, the first six eigenmodes are also given in Fig. 13 and compared to the results obtained by the FEM with a remarkable agreement.

5. Conclusion

Natural frequency analysis of classical plates by a novel mesh-free method has been reported. Different complicated geometrical shapes of Kirchhoff plates are successfully examined in terms of free vibration investigation. Several numerical examples dealt with both regular and irregular nodal distributions are considered and their results obtained are then compared with each other as well as other available approaches. A good agreement is found evidently. As a result, it successfully demonstrated the applicability and the effectiveness of the proposed method in natural frequency analysis of plate structures with complicated shape. The studies have confirmed that the choice of both the correlation parameter and the scaling factor is totally dependent upon the problems of interest. In the study, $2 \leq \alpha \leq 4$ and $1 \leq \theta \leq 100$ must be chosen in practice so that a reasonable solution can be obtained. Nevertheless, it can be consequently claimed that the technique is robust, efficient, and accurate. Application of the method for other problems such as laminated composite, piezoelectric, magnetoelectroelastic materials, crack problems, etc., is generally possible. The fully clamped boundary condition could be developed by two possibilities, whether applied by a Hermite-type form based approximation technique introduced by Liu *et al.* [2006], Cui *et al.* [2009], or smoothed techniques by Cui *et al.* [2010].

References

Abbassian, F., Dawswell, D. J. and Knowles, N. C. [1987] *Free Vibration Benchmarks* (Atkins Engineering Sciences, Glasgow).

Atluri, S. N. [2004] *The Meshless Local Petrov–Galerkin (MLPG) Method* (Tech. Science Press).

Atluri, S. N. and Zhu, T. [1998] "A new meshless local Petrov–Galerkin (MLPG) approach in computational mechanics," *Comput. Mech.* **22**, 117–127.

Belytschko, T., Lu, Y. Y. and Gu, L. [1994] "Element free Galerkin method," *Int. J. Numer. Meth. Eng.* **37**, 229–256.

Belyschko, T., Organ, D. and Krongauz, Y. [1995] "A coupled finite element — element free Galerkin method," *Comput. Mech.* **17**, 186–195.

Belytschko, T. and Black, T [1999] "Elastic crack growth in finite elements with minimal remeshing," *Int. J. Numer. Meth. Eng.* **45**, 601–620.

Bui, Q. T. [2005] "Application of the element free Galerkin method for dual analysis," European Master's thesis, EMMC, University of Liege, Belgium.

Bui, Q. T. and Nguyen-Dang, H. [2006] "An equilibrium model in the element free Galerkin method," *Proc. Eight Int. Conf. Computational Structures Technology*, Las Palmas de Gran Canaria, Spain, pp. 12–15.

Bui, Q. T., Nguyen, N. T. and Nguyen-Dang, H. [2009] "A moving Kriging interpolation-based meshless method for numerical simulation of Kirchhoff plate problems," *Int. J. Numer. Meth. Eng.* **77**, 1371–1395.

Chen, J. T., Chen, I. L., Chen, K. H., Lee, Y. T. and Yeh, Y. T. [2004] "A meshless method for free vibration analysis of circular and rectangular clamped plates using radial basis function," *Eng. Anal. Bound. Elem.* **28**, 535–545.

Cui, X., Liu, G. R. and Li, G. [2009] "A smoothed Hermite radial point interpolation method for thin plate analysis," *Arch. Appl. Mech.*, doi: 10.1007/s00419-009-0392-0.

Cui, X. Y., Liu, G. R., Li, G. Y. and Zhang, G. Y. [2010] "Thin plate formulation without rotation DOFs based on radial point interpolation method," *Int. J. Numer. Meth. Eng.*, doi: 10.1002/nme.3000.

Dai, K. Y., Liu, G. R., Lim, M. K. and Gu, Y. T. [2003] "Comparison between the radial point interpolation and the Kriging interpolation used in mesh-free method," *Comput. Mech.* **32**, 60–70.

Duflot, M. and Nguyen-Dang, H. [2002] "Dual analysis by a meshless method," *Commun. Numer. Meth. Eng.* **18**, 621–631.

Giunta, A. A. and Watson, L. T. [1998] "A comparison of approximation modeling techniques: Polynomial versus interpolating models," *Multidisciplinary Analysis and Design (MAD) Center for Advanced Vehicles, Virginia 2406.* AIAA–4758.

Gu, L. [2003] "Moving Kriging interpolation and element free Galerkin method," *Int. J. Numer. Meth. Eng.* **56**, 1–11.

Krysl, P. and Belytschko, T. [1995] "Analysis of thin plates by the element-free Galerkin method," *Comput. Mech.* **17**, 26–35.

Lam, K. Y., Wang, Q. X. and Li, H. [2004] "A novel meshless approach — Local Kriging (LoKriging) method with two-dimensional structural analysis," *Comput. Mech.* **33**, 235–244.

Leitão, A. V. M. [2001] "A meshless method for Kirchhoff plate bending problems," *Int. J. Numer. Meth. Eng.* **52**, 1107–1130.

Li, H., Wang, Q. X. and Lam, K. Y. [2004] "Development of a novel meshless Local Kriging (LoKriging) method for structural dynamic analysis," *Comput. Meth. Appl. Mech. Eng.* **193**, 2599–2619.

Li, S. and Liu, W. K. [2004] *Mesh-free Particles Methods* (Springer Berlin Heidelberg, New York, Germany).

Liew, K. M., Huang, Y. Q. and Reddy, J. N. [2004] "Analysis of general shaped thin plates by the moving least-squares differential quadrature method," *Finit. Elem. Anal. Design* **40**, 1453–1474.

Liew, K. M. and Liu, F. L. [1997] "Differential cubature method: A solution technique for Kirchhoff plates of arbitrary shape," *Comput. Meth. Appl. Mech. Eng.* **145**, 1–10.

Liu, G. R. [2003] *Mesh-free Methods, Moving Beyond the Finite Element Method* (CRC Press, USA).

Liu, G. R. and Chen, X. L. [2001] "A mesh-free method for static and free vibration analyses of thin plates of complicated shape," *J. Sound Vibr.* **241**, 839–855.

Liu, Y., Hon, Y. C. and Liew, K. M. [2006] "A mesh-free Hermite-type radial point interpolation method for Kirchhoff plate problems," *Int. J. Numer. Meth. Eng.* **66**, 1153–1178.

Melenk, J. M. and Babuska, I. [1996] "The partition of unity finite element method: Basic theory and applications," *Comput. Meth. Appl. Mech. Eng.* **139**, 289–314.

Moes, N., Dolbow, J. and Belytschko, T. [1999] "A finite element method for crack growth without remeshing," *Int. J. Numer. Meth. Eng.* **46**, 131–150.

Nguyen, N. T. [2007] "A meshless Kriging method for thin plate bending," European Master's thesis, EMMC, University of Liege, Belgium.

Sayakoummane, V. and Kanok-Nukulchai, W. [2007] "A meshless analysis of shells based on moving Kriging interpolation," *Int. J. Comput. Meth.* **4**, 543–565.

Simkins, D. C. Jr., Li, S., Lu, H. and Liu, W. K. [2004] "Reproducing kernel element method. Part IV: Globally compatible C^n $(n \geq 1)$ triangular hierarchy," *Comput. Meth. Appl. Mech. Eng.* **193**, 1013–1034.

Sladek, J., Sladek, V. and Mang, H. M. [2003] "Meshless LBIE formulations for simply supported and clamped plates under dynamic load," *Comput. Struct.* **81**, 1643–1651.

Tongsuk, P. and Kanok-Nukulchai, W. [2004a] "On the parametric refinement of moving Kriging interpolations for element free Galerkin method," *Computational Mechanics WCCM VI in Conjunction with APCOM'04*, Sept. 5–10, Beijing, China.

Tongsuk, P. and Kanok-Nukulchai, W. [2004b] "Further investigation of element free Galerkin method using moving Kriging interpolation," *Int. J. Comput. Meth.* **1**, 1–21.

Zhou, D. and Ji, T. [2006] "Free vibration of rectangular plates with continuously distributed spring-mass," *Int. J. Sol. Struct.* **43**, 6502–6520.